THE ASTROPHYSICAL JOURNAL, 549:948–958, 2001 March 10

TIDAL SPIN-UP OF STARS IN DENSE STELLAR CUSPS AROUND MASSIVE BLACK HOLES

TAL ALEXANDER AND PAWAN KUMAR
Institute for Advanced Study, Olden Lane, Princeton, NJ 08540
Received 2000 April 13; accepted 2000 November 9

ABSTRACT

We show that main-sequence stars in dense stellar cusps around massive black holes are likely to rotate at a significant fraction of the centrifugal breakup velocity as a result of spin-up by hyperbolic tidal encounters. We use realistic stellar structure models to calculate analytically the tidal spin-up in soft encounters and extend these results to close and penetrating collisions using smoothed particle hydrodynamics simulations. We find that the spin-up effect falls off only slowly with distance from the black hole because the increased tidal coupling in slower collisions at larger distances compensates for the decrease in the stellar density. We apply our results to the stars near the massive black hole in the Galactic center. Over their lifetime, $\sim 1\ M_\odot$ main-sequence stars in the inner 0.3 pc of the Galactic center are spun-up on average to $\sim$10%–30% of the centrifugal breakup limit. Such rotation is $\sim$20–60 times higher than is usual for such stars and may affect their subsequent evolution and their observed properties.

Subject headings: Galaxy: center — Galaxy: kinematics and dynamics — galaxies: nuclei — stars: kinematics — stars: rotation

On-line material: color figures

1. INTRODUCTION

It is now widely accepted that supermassive black holes (BHs) exist in many, if not all, galactic centers (Magorrian et al. 1998). Dynamical models of the evolution of such systems generically predict the formation of a dense stellar cusp near the BH (e.g., Bahcall & Wolf 1977; Young 1980). Stars moving rapidly in the dense stellar cusp near the BH will suffer numerous high-velocity close tidal encounters over their lifetimes. Although such encounters transfer some energy and angular momentum from the hyperbolic orbit to the colliding stars, they rarely remove enough energy for tidal capture. This is in marked contrast to the situation in the high-density cores of globular clusters, where the colliding stars are on nearly zero-energy orbits and close collisions lead to the formation of tight binaries. The effects of hyperbolic encounters on the stars are mostly transient. The dynamical and thermal relaxation timescales are very short compared to the stellar lifetime, and thus apart from some mass loss in very close collisions, the star is largely unaffected. It is, however, more difficult for the star to shed the excess angular momentum since magnetic breaking operates on timescales of the order of the stellar lifetime (Gray 1992). High rotation is therefore the longest lasting dynamical aftereffect of a close encounter.

The possibility that stars in BH cusps are rapid rotators may have interesting implications for their evolution and the interpretation of their observed properties. The effects of rotation and rotationally induced mixing in a main-sequence (MS) star on its subsequent evolution have been studied by Sweigart (1997) and Vandenberg, Larson, & De Propris (1998) in the context of globular clusters, without specifying the origin of the rotation, and by Sills, Pinsonneault, & Terndrup (2000) in the context of young open clusters. Rotationally induced mixing may reveal itself in the spectral line ratios, and rotation may be directly observed in the spectral line profiles. Detection of such signatures in the spectra of the observed giants can provide additional evidence for the existence of an underlying cusp of MS stars, which at present cannot be directly observed.

The goal of this study is to estimate the magnitude of the tidal spin-up, with particular emphasis on the Galactic center (GC). Present-day observations can already resolve individual giant stars very close to the BH in the GC (Genzel et al. 1997; Ghez et al. 1998), and high-resolution infrared spectroscopy is possible for the brighter giants (Carr, Sellgren, & Balachandran 2000; Ramirez et al. 2000). The depletion of luminous giants in the inner 2″ ($\sim$0.1 pc) around the supermassive BH in the GC was interpreted by Alexander (1999) as evidence for collisional destruction in an extreme density of a sharp stellar cusp. It is inevitable that where the stellar density is high enough to destroy giants, smaller stars that escape destruction will suffer very close collisions. The inner GC is therefore a promising environment for studying the spin-up effect.

The paper is organized as follows. In § 2 we present the formalism for spin-up in the linear regime of soft hyperbolic encounters. In § 3 we discuss results from smoothed particle hydrodynamics (SPH) simulations of nonlinear close encounters and incorporate them in our spin-up calculations. In § 4 we calculate the spin-up of stars in the inner parsec of the GC. We discuss and summarize our results in § 5. An appendix describes the analytic calculation of the tidal coupling constants for hyperbolic encounters using realistic stellar structure models of an MS dwarf and of a giant.

2. SPIN-UP BY SOFT HYPERBOLIC TIDAL ENCOUNTERS

2.1. *Stochastic Spin-up in the Linear Regime*

We begin by considering soft (distant) encounters where the tidal deformations are small enough to be treated as linear perturbations. We consider the effect of the tides raised by an impactor star of mass m on a target star of mass M and radius R as the impactor follows an unbound orbit with a periseparation r_p from the target star. We will use the tilde symbol to denote mass in terms of M, distances in terms of R, time in terms of $(R^3/GM)^{1/2}$, velocity in terms of the Keplerian velocity $(GM/R)^{1/2}$, energy in terms of GM^2/R, angular momentum in terms of $(GM^3R)^{1/2}$, and

TABLE 1

PARAMETERS OF REPRESENTATIVE MS AND GIANT STARS

Type	M ($M_\odot$)	R ($R_\odot$)	V_e (km s^{-1})	V_k (km s^{-1})	$V_{\rm obs}$ (km s^{-1})	K (mag)	T (yr)	$\tilde{I}$	$\tilde{E}_b$
K2(V).....	0.76	0.75	621	440	~ 2	~ 22	$>10^{10}$	0.07	1.65
G5(III).....	2.4	8	340	240	~ 5	~ 16	1.6×10^8	0.13	6.11
$n = 1.5$.....	...	...	...	...	...	...	...	0.21	0.85

NOTE.—The parameters of representative MS and giant stars (Zombeck 1990; Lang 1991). The mean observed equatorial circular velocity $V_{\rm obs}$ is from Gray 1992. Over the time T, the star is as bright or brighter than the quoted apparent K magnitude (for stars in the GC, $\Delta = 14.5^{\rm m}$, $A_K = 3.5^{\rm m}$) and has a radius as large or larger than the quoted value (based on the twice solar metallicity stellar tracks of Schaerer et al. 1993). The moment of inertia $\tilde{I}$ and the binding energy $\tilde{E}_b$ were estimated from stellar structure models of the Sun (Christensen-Dalsgaard et al. 1996) and the αUMa giant ($M = 4.25\ M_\odot$, $R = 27.4\ R_\odot$; Guenther et al. 2000). For comparison, $\tilde{I}$ and $\tilde{E}_b$ for an ideal gas $n = 1.5$ polytrope are also listed.

moment of inertia in terms of MR^2. In these units $\tilde{\Omega} = 1$ is the centrifugal breakup angular frequency. A star with $\tilde{\Omega} > 1$ will shed mass from its equator as a result of the centrifugal force.

We describe the results in the reduced mass system where the target star is at the origin. The angular momentum $\Delta\tilde{L}$ that is transferred from the orbit to the target star is related to the deposited tidal energy $\Delta\tilde{E}$ by (Goldreich & Nicholson 1989; Kumar & Quataert 1998)

$$\Delta\tilde{E} = \Delta\tilde{L}\tilde{\Omega}_p\,, \tag{1}$$

where $\tilde{\Omega}_p$ is the angular velocity at periastron. The energy invested in raising the tides is given in the linear regime by (Press & Teukolsky 1977)

$$\Delta\tilde{E} = \frac{\tilde{m}^2}{\tilde{r}_p^2}\sum_{l=2}^{\infty}\frac{T_l(\eta)}{\tilde{r}_p^{2l}}\,, \tag{2}$$

where the tidal coupling coefficients T_l depend on the structure of the star and the eccentricity of the orbit and are functions of the parameter η,

$$\eta = \sqrt{\frac{\tilde{r}_p^3}{1+\tilde{m}}}\,. \tag{3}$$

For rigid body rotation,[1] the change in the star's angular momentum is related to the change in the angular velocity $\Delta\tilde{\Omega}$ by the star's moment of inertia $\tilde{I}$,

$$\Delta\tilde{L} = \tilde{I}\Delta\tilde{\Omega}\,. \tag{4}$$

In the case of differential rotation, $\Delta\tilde{\Omega}$ is defined by equation (4) and is the effective angular velocity. The spin-up of the target star in a single tidal encounter can therefore be expressed as

$$\Delta\tilde{\Omega} = \frac{\tilde{m}^2}{\tilde{I}\tilde{\Omega}_p\tilde{r}_p^2}\sum_{l=2}^{\infty}\frac{T_l(\eta)}{\tilde{r}_p^{2l}}\,, \tag{5}$$

where it is assumed that the star maintains its original moment of inertia. The periastron angular velocity is related to the relative velocity at infinity, $\tilde{v}_\infty$, by

$$\tilde{\Omega}_p^2 = \frac{\tilde{v}_\infty^2}{\tilde{r}_p^2} + \frac{2(1+\tilde{m})}{\tilde{r}_p^3}\,, \tag{6}$$

where the second term expresses the enhancement due to gravitational focusing.

[1] The timescale for angular momentum redistribution due to convective transport in a late-type giant is ~ 1 yr (Zahn 1989), and so rigid rotation is achieved on a timescale similar to that of the collision itself. The timescale for angular momentum redistribution in radiative MS stars is not well known, although it is likely to be shorter than the stellar lifetime.

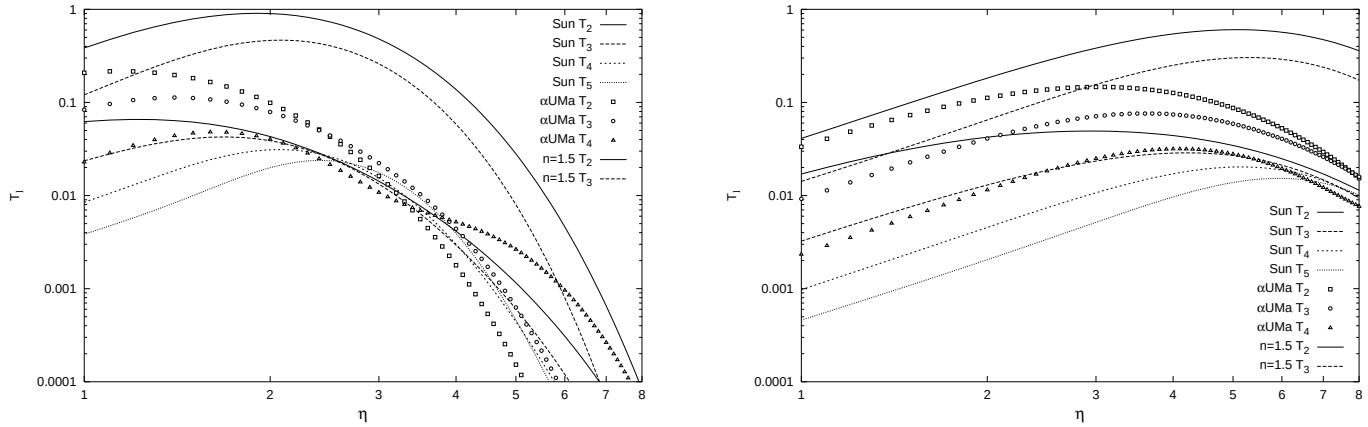

FIG. 1.—First few orders of T_l for the solar stellar structure model, the giant model, and the ideal gas $n = 1.5$ polytrope. *Left:* Parabolic ($e = 1$) orbits. *Right:* Hyperbolic ($e = 10$) orbits.

Many encounters at random orientations lead to a "random walk" buildup of the stellar spin. Over the stellar lifetime $\tilde{T}$, the rms change in the stellar angular velocity is given by adding in quadrature the contributions from collisions with different values of the periseparation $\tilde{r}_p$ and of the orbital energy $\tilde{E}_o$, weighted by the differential collision rate $d^2\tilde{q}/d\tilde{r}_p\, d\tilde{E}_o$,

$$\delta\tilde{\Omega} \equiv \langle \Delta\tilde{\Omega}^2 \rangle^{1/2} = \left(\tilde{T} \int d\tilde{r}_p \int d\tilde{E}_o\, \Delta\tilde{\Omega}^2\, \frac{d^2\tilde{q}}{d\tilde{r}_p\, d\tilde{E}_o} \right)^{1/2} . \tag{7}$$

The differential rate is calculated with the approximation that the relative velocity can be described by the Maxwellian distribution function (DF) with a mass-independent one-dimensional velocity dispersion $\tilde{\sigma}_2^2 = 2\tilde{\sigma}^2$ (§ 4.1),

$$\frac{d^2\tilde{q}}{d\tilde{r}_p\, d\tilde{E}_o} = \frac{\sqrt{8\pi}\tilde{n}}{\tilde{\mu}^2\tilde{\sigma}_2^3} \exp\left(-\frac{\tilde{E}_o}{\tilde{\mu}\tilde{\sigma}_2^2} \right) (2\tilde{r}_p \tilde{E}_o + \tilde{m}) , \tag{8}$$

where $\tilde{n}$ is the space density of the impactors. This estimate involves the approximation that the angular momentum transfer does not depend on whether the star is rotating in a prograde or retrograde sense with respect to the orbit, and it assumes that the mass loss and the change in the star's structure and moment of inertia can be neglected. Because $\Delta\tilde{\Omega}^2 \sim \tilde{r}_p^{-9}$ whereas $d^2\tilde{q}/d\tilde{r}_p\, d\tilde{E}_o \sim \tilde{r}_p$, the rms $\delta\tilde{\Omega}$ is dominated by the collisions with the smallest $\tilde{r}_p$. When the stellar population includes a spectrum of masses, $\int f_{\tilde{m}}\, d\tilde{m} = 1$, the average spin-up is obtained by adding the weighted contributions in quadrature,

$$\delta\tilde{\Omega} \equiv \left\langle \int d\tilde{m} f_{\tilde{m}}\, \Delta\tilde{\Omega}^2 \right\rangle^{1/2} . \tag{9}$$

2.2. *Linear Tidal Coupling Coefficients*

The orbital energy $\tilde{E}_o$ is related to $\tilde{v}_\infty$ and the eccentricity of the orbit e by

$$\tilde{E}_o = \frac{1}{2}\, \tilde{\mu}\tilde{v}_\infty^2 = \frac{1}{2}\, \tilde{\mu}\, \frac{e-1}{\tilde{r}_p} , \tag{10}$$

where $\tilde{\mu} = \tilde{m}/(1+\tilde{m})$ is the reduced mass. The eccentricity that corresponds to the mean orbital energy (eq. [21] below) is

$$\langle e \rangle = 6\tilde{r}_p\, \tilde{\sigma}^2 + 1 . \tag{11}$$

Since e can reach very high values when $\tilde{\sigma} \gg 1$, as is the case for giants (low Keplerian velocity) close to the BH, it is necessary to extend the standard ($e = 1$) tidal interaction formalism of Press & Teukolsky (1977) to hyperbolic orbits. This is described in Appendix A.

In this work we consider two types of target stars: an MS dwarf and a red giant, whose properties are summarized in Table 1. The detailed stellar structures that we use to calculate the tidal coupling coefficients for these stars are based on the solar model of Christensen-Dalsgaard et al. (1996) and a model for the red giant αUMa (Guenther et al. 2000). Figure 1 shows the run of T_l with η for the two stars and for an ideal gas $n = 1.5$ polytrope, for parabolic ($e = 1$) and hyperbolic ($e = 10$) orbits. We find that the tidal coupling in an ideal gas polytrope is stronger than in either of the more realistic models. We also find a general trend for the T_l coefficients to reach their maxima at larger values of η (larger $\tilde{r}_p$ for a given $\tilde{m}$) with increasing e (and increasing periastron velocity $\tilde{v}_p$). This reflects the fact that the coupling is strongest when $\tilde{\Omega}_p = \tilde{v}_p/\tilde{r}_p$ equals the lowest frequency stellar pulsation mode.

3. SPIN-UP BY STRONG HYPERBOLIC COLLISIONS

3.1. *SPH Simulations*

In order to extend the linear treatment of the soft encounters to strong (close and penetrating) encounters, we simulated such encounters with the SPH technique (Lucy 1977; Gingold & Monaghan 1977). In view of the difficulty of simulating all the aspects of a real stellar collision, and in view of the many uncertainties in the details of the stellar structure, the purpose of these simulations is not to calculate $\Delta\tilde{\Omega}$ precisely for specific collisions but rather to gain *qualitative* insight about angular momentum transfer in strong encounters, which can then be incorporated in our semianalytic calculations by simple approximations. The SPH code we use calculates the gravitational force by direct N^2 operations and is therefore limited to relatively low resolution simulations (typically $N = 2048$ particles). The code integrates in time the entropy equation (Hernquist 1993), conserves particle momenta identically, uses the symmetrized W_4 spline kernel (Monaghan & Lattanzio 1985) with an adaptive smoothing length that is adjusted always to include 40 neighboring particles, and uses the artificial viscosity prescription given by Hernquist & Katz (1989, eqs. [2.22], [2.23], and [2.37]) and the time step criteria of Katz, Weinberg, & Hernquist (1996). The amount of stellar mass loss in the collisions is estimated by the enthalpy criterion of Rasio & Shapiro (1991).

We verified the code by constructing stable $n = 1.5$ polytrope configurations, by confirming that the results converge as the number of particles is increased, and by reproducing qualitatively the spin-up and mass loss obtained in the SPH simulations of Davies, Benz, & Hills (1991), who used a much more realistic stellar structure model. Of direct relevance is the fact that our SPH code reproduces the results of the linear theory at the soft collision limit ($\tilde{r}_p \gtrsim 2.5$) and at smaller $\tilde{r}_p$ follows closely the SPH results obtained by Rasio & Shapiro (1991) (Fig. 2) in SPH simulations with 10^4 particles.

3.2. *Beyond the Linear Regime*

3.2.1. *Deep Inelastic Collisions*

At small periseparations (small η for fixed $\tilde{m}$), the sum in equation (5) converges slowly and the truncation of the T_l series at some order $l = k$ could underestimate $\Delta\tilde{\Omega}$. We make use of the fact that the ratio $T_{l+1}(\eta)/T_l(\eta)$ is roughly constant (Fig. 1) over the small-η range of interest to extrapolate the sum to high l by a geometric series

$$\Delta\tilde{\Omega} \approx C_{\rm NL}\, \frac{\tilde{m}^2}{\tilde{I}\tilde{\Omega}_p \tilde{r}_p^2} \left[\sum_{l=2}^{k-2} \frac{T_l}{\tilde{r}_p^{2l}} + \frac{T_{k-1}}{\tilde{r}_p^{2k-2}} \left(1 - \frac{T_k}{\tilde{r}_p^2\, T_{k-1}} \right)^{-1} \right] , \tag{12}$$

where the constant $C_{\rm NL}$ is a nonlinear correction factor, which we calibrate by the SPH simulations as discussed below. Figure 2 compares the prediction of the linear theory with the numeric SPH results without correcting for nonlinear effects ($C_{\rm NL} = 1$). While the two agree at the limit of soft (distant) encounters, $\Delta\tilde{E}$ grows faster than the linear theory at close encounters. In this particular example the high-order correction is very small and does not exceed 2% down to $\tilde{r}_p = 1.6$.

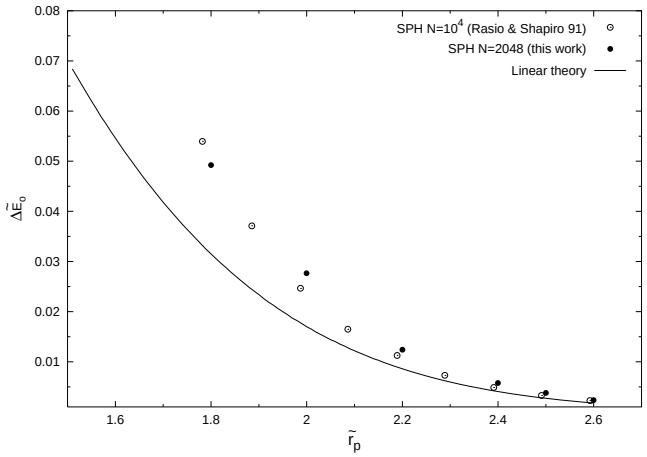

FIG. 2.—Energy transferred from the orbit to the star in a parabolic collision between a point mass and an ideal gas $n = 1.5$ polytrope of equal mass ($\tilde{m} = 1$, $\tilde{E}_o = 0$) as a function of the periseparation $\tilde{r}_p$. The SPH results from this work are compared with the higher resolution SPH results of Rasio & Shapiro (1991) and with the predictions of the linear theory (eq. [12] with $C_{\rm NL} = 1$).

Figures 3 and 5 show snapshots from two SPH simulations of extremely nonlinear collisions. Figure 4 shows the run of the dynamical properties of the target star with $\tilde{r}_p$ in $\tilde{m} = 1$, $\tilde{E}_o = 2$ collisions. Our analytic expressions for $\Delta\tilde{L}$ and $\Delta\tilde{\Omega}$ consistently underestimate the SPH results for a point mass impactor by a factor of ~ 3 down to $\tilde{r}_p \sim 1.5$. Similarly, it underestimates $\Delta\tilde{E}$ in parabolic collisions by a factor of ~ 1.5 at $\tilde{r}_p = 1.8$ (Fig. 2). We find that at smaller periseparations where significant amounts of mass are ejected in the collisions, a large fraction of the angular momentum that is taken out of the orbit is deposited in the ejecta rather than in the target star. This truncates the $\Delta\tilde{\Omega} \sim \tilde{r}_p^{-5}$ divergence and limits the spin-up efficiency, so that the difference between the analytic calculations and simulation results decreases with $\tilde{r}_p$ until the two cross over. We approximate the decrease in spin-up efficiency by introducing a truncation periseparation $\tilde{r}_0$ such that $\Delta\tilde{\Omega}(\tilde{r}_p) = \Delta\tilde{\Omega}(\tilde{r}_0)$ for $\tilde{r}_p < \tilde{r}_0$.

We now discuss our choice of $\tilde{r}_0$. Figure 4 shows that $\Delta\tilde{\Omega}$ is much more suppressed than $\Delta\tilde{L}$ at small $\tilde{r}_p$ because the stellar moment of inertia increases as a consequence of the

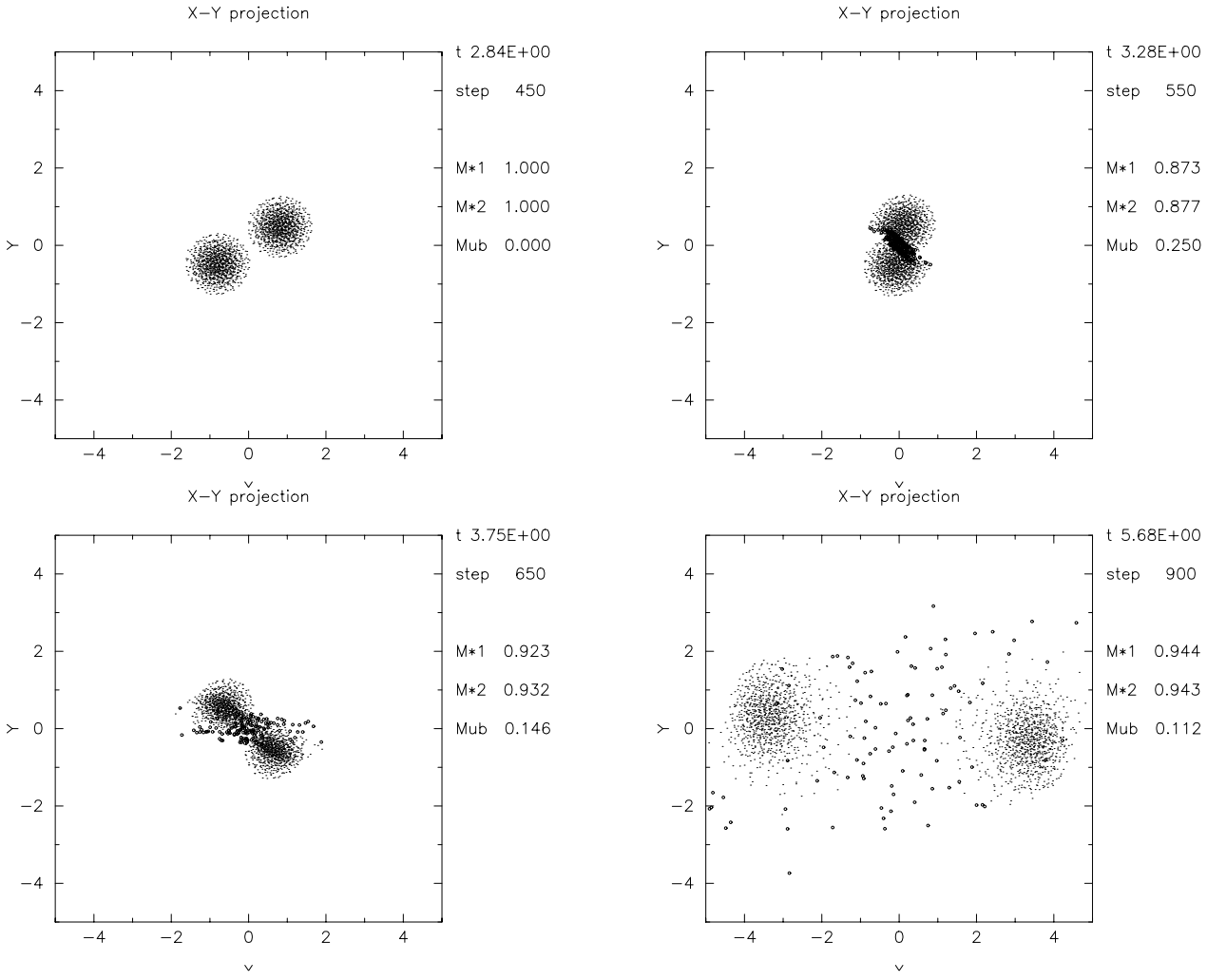

FIG. 3.—Sequence of snapshots from an SPH simulation of a deep collision between two equal-mass stars (modeled as ideal gas $n = 1.5$ polytropes with $N = 1024$ particles each). The dots represent SPH gas particles that remain bound to the stars, and the circles represent those that are lost. The orbital parameters of the encounter are $\tilde{r}_p = 1.0$ and $\tilde{E}_o = 2$. At $\tilde{t} = 20$ after the periastron passage (not shown here), the stars lost 5% of their mass each, were spun-up by $\Delta\tilde{\Omega} = 0.025$, and acquired a moment of inertia $\tilde{I} = 0.47$, more than twice the initial value. [*See the electronic edition of the Journal for a color version of this figure.*]

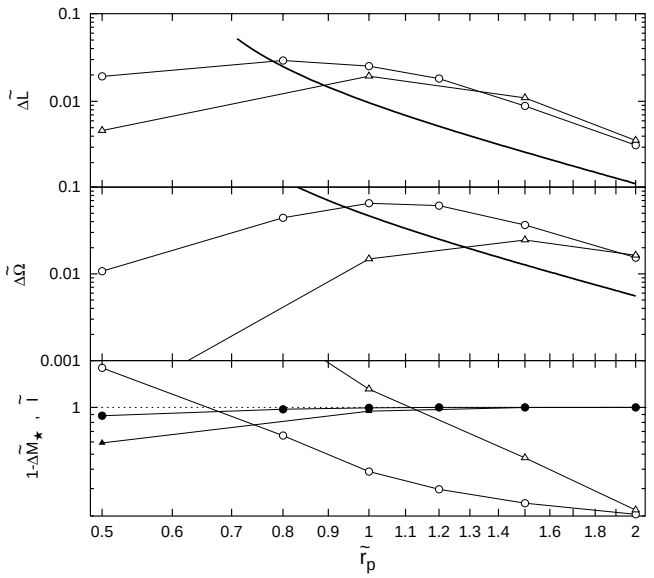

FIG. 4.—Response of a star ($\tilde{m} = 1$, modeled as an ideal gas $n = 1.5$ polytrope) to deep nonlinear hyperbolic collisions ($\tilde{E}_o = 2$) with another star, for both the case in which the impactor (modeled as a point mass) is compact relative to the target star (*circles*) and the case in which the impactor (modeled as an ideal gas $n = 1.5$ polytrope) is of the same size as the target star (*triangles*). The SPH results (*thin lines with symbols*) are compared with the analytic calculations without the nonlinear correction (*thick lines*) for $\Delta\tilde{L}$ (*top panel*) and $\Delta\tilde{\Omega}$ (*middle panel*). Also shown in the bottom panel are $1 - \Delta\tilde{M}_*$, the mass that remains bound to the star after the collision (*thin lines with filled symbols*), and $\tilde{I}$, the star's moment of inertia after the collision (*thin lines with open symbols*).

collision. The increase in $\tilde{I}$ far exceeds the small change that is expected as a result of the stellar oblateness that develops in response to the rotation. The effect seen in the simulation is due to the heating and subsequent expansion of the star by the collision. Our SPH models do not include the radiative processes that are necessary for describing the later stages of cooling and contraction. It is therefore likely that the final value of $\Delta\tilde{\Omega}$ is not as strongly suppressed as is implied by Figure 4 but rather follows more closely the behavior of $\Delta\tilde{L}$. A collision with an impactor of a size comparable to that of the target results in much more mass loss than a collision with an impactor that is effectively a point mass (e.g., a stellar remnant on an MS star or an MS star on a giant). However, it is likely that the SPH results overestimate the mass loss since an $n = 1.5$ polytrope has a significantly lower binding energy than the realistic stellar structure models on which we base our analytic calculations (Table 1). Figure 4 shows that the analytic estimate of $\Delta\tilde{\Omega}$ equals the value derived from the simulation at $\tilde{r}_p \sim 1.3$ and $\tilde{r}_p \sim 0.9$ for polytrope and point mass impactors, respectively. For $\Delta\tilde{L}$ the analytic estimate and the simulation results are equal at $\tilde{r}_p \sim 0.9$ and $\tilde{r}_p \sim 0.8$, respectively. Based on the arguments presented above, we adopt in this work the simple prescription that $\tilde{r}_0 = 1.0$ or the size of the impactor, whichever is larger, for all types of collisions. We note that the analytic calculations still *underestimate* the SPH results by a factor of 2 at $\tilde{r}_p = \tilde{r}_0$ and by a factor of 3 at $\tilde{r}_p = 2$. A difference of a similar magnitude is seen also in parabolic collisions (Fig. 2). We compensate for this discrepancy by setting the nonlinear correction factor to $C_{\rm NL} = 2$. A more extensive investigation of parameter space by SPH simulations with more realistic stellar structure models will be required to refine this prescription.

3.2.2. *Prompt Disruption of Tidally Formed Binaries*

Close hyperbolic encounters of stars in the low-energy tail of the orbital energy distribution can lead to the formation of a bound system ($\tilde{E}_o + \Delta\tilde{E}_o < 0$) with a large semimajor axis $\tilde{a}$. Although such encounters are very efficient in spinning-up stars, the subsequent evolution of the stellar rotation in binaries is very different from that due to stochastic encounters. We do not consider such cases in this work, and they are not included in the average $\delta\tilde{\Omega}$ (eq. [9]). Because of the very large stellar density and the proximity of the massive BH, it is necessary to check whether a newly formed binary can survive its first orbital period without being disrupted by a tidal interaction with either a third nearby star or the central BH.

We take this into account by considering the orbit as bound only if the change in the orbital angular momentum, $\Delta\tilde{L}_{\rm orb}$, due to the torque exerted on the system by the third mass $\tilde{m}_3$ (star or central BH) is smaller than the orbital angular momentum $\tilde{L}_{\rm orb}$,

$$\Delta\tilde{L}_{\rm orb} = 4\pi\left(\frac{\tilde{a}}{\tilde{d}}\right)^3\left(\frac{\tilde{m}_3}{1+\tilde{m}}\right)(1-e^2)^{-1/2}\tilde{L}_{\rm orb}\,, \qquad (13)$$

where $\tilde{d}$ is the distance of $\tilde{m}_3$ from the binary and where we used the relation $\tilde{L}^2_{\rm orb} = \tilde{m}\tilde{\mu}\tilde{a}(1-e^2)$. For disruption by a star, $d \sim \tilde{n}^{-1/3}$, $\tilde{m}_3 \sim \tilde{m}$, and the no-disruption criterion is

$$4\pi\tilde{n}\tilde{a}^3\tilde{\mu}(1-e^2)^{-1/2} < 1\,. \qquad (14)$$

The eccentricity and the semimajor axis are estimated from the unperturbed periseparation and the bound orbit's energy

$$e = \frac{2(\tilde{E}_o + \Delta\tilde{E}_o)}{\tilde{\mu}}\,\tilde{r}_p + 1\,, \quad \tilde{a} = \frac{\tilde{r}_p}{1-e}\,. \qquad (15)$$

In practice, we find that the contribution from disrupted binaries to $\delta\tilde{\Omega}$ in the GC is negligible.

3.2.3. *Tidal and Collisional Destruction*

The precise criterion for tidal destruction of stars by hyperbolic encounters is not well known. In this work we adopt the simple criterion that tidal breakup occurs when $\Delta\tilde{v}$, the change in the velocity of a mass element on the stellar surface, exceeds the escape velocity, $\Delta\tilde{v} \sim (2\tilde{m}/\tilde{r}_p^3)(\tilde{r}_p/\tilde{v}_p) > \sqrt{2}$. The tidal radius $\tilde{r}_t$ is a function of the impactor mass and orbital energy and is given by the solution to the equation

$$\tilde{r}_t = \left(\frac{\tilde{\mu}\tilde{m}}{\tilde{m} + \tilde{r}_t\tilde{E}_o}\right)^{1/3}\tilde{m}^{1/3}\,. \qquad (16)$$

Our SPH simulations indicate that this is a conservative criterion. Figure 5 shows a sequence of snapshots from an encounter with $\tilde{r}_p = \tilde{r}_t = 2.0$, $\tilde{E}_o = 1.0$ between an $\tilde{m} = 10$ black hole (modeled as a point mass) and an MS dwarf (modeled as an ideal gas $n = 1.5$ polytrope). The star survives the collision after suffering $\sim$25% mass loss. We performed several spot checks with different values of $\tilde{r}_p$ and $\tilde{E}_o$ and verified that this prescription for $\tilde{r}_t$ indeed roughly demarcates the boundary where the fractional mass loss increases to order unity and that $\Delta\tilde{\Omega}$ significantly exceeds the value predicted by our extrapolated linear formalism for such deep collisions.

When $\tilde{r}_t < 1$ (point mass impactor) or $\tilde{r}_t < 2$ (impactor of same size as the target), it is necessary to consider the possibility of collisional destruction. Our SPH simulations indicate that the $n = 1.5$ polytrope stellar models can survive

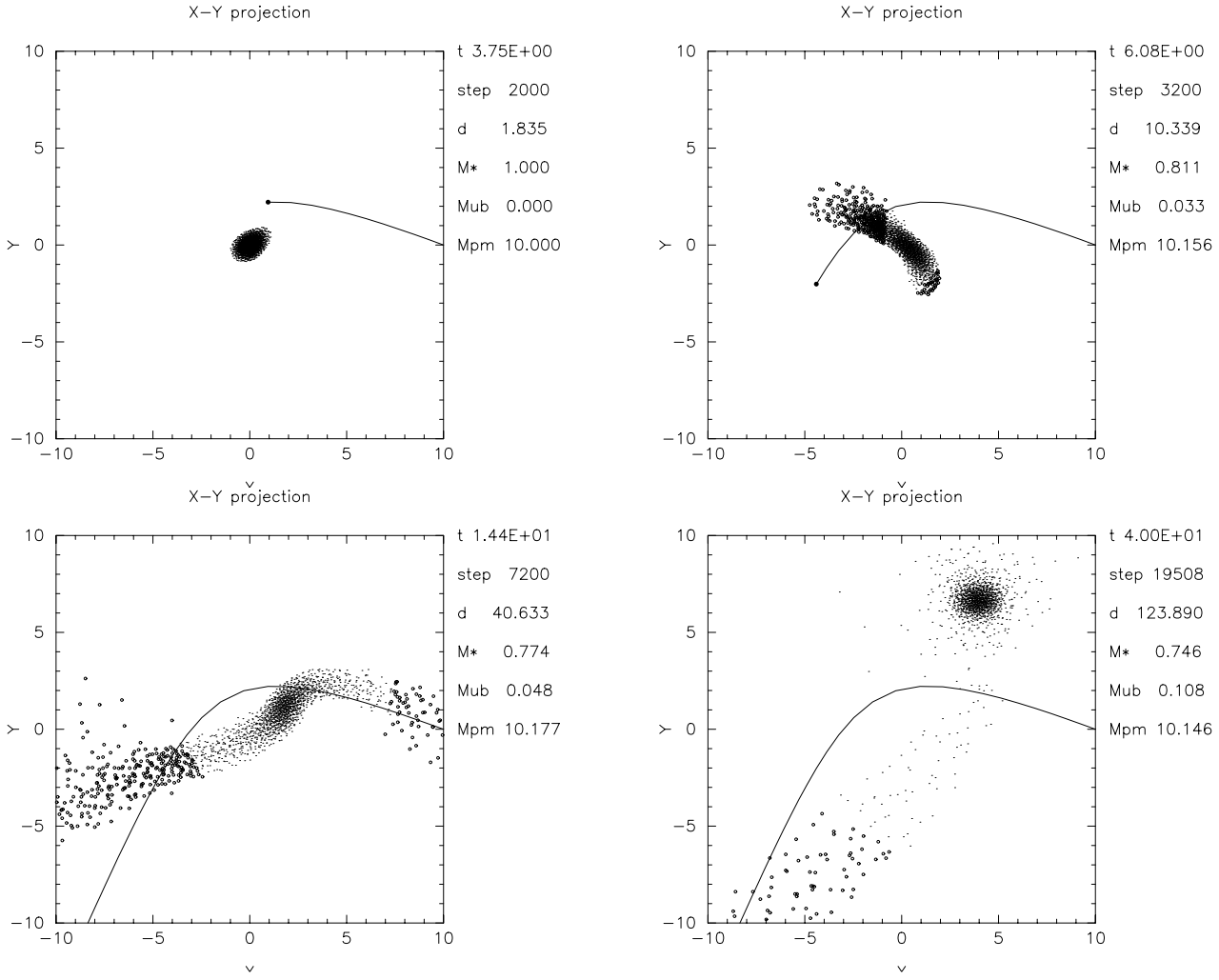

FIG. 5.—Sequence of snapshots from an SPH simulation of a collision at the tidal limit (eq. [16]) between an $\tilde{m} = 10$ BH (modeled as a point mass) and an MS star (modeled as an ideal gas $n = 1.5$ polytrope). The dots represent SPH gas particles that remain bound to the star, and the circles represent those that are lost. The line traces the trajectory of the BH in a frame where the target was initially at rest. The orbital parameters of the encounter are $\tilde{r}_p = \tilde{r}_t = 2.0$ and $\tilde{E}_o = 1.0$. In spite of the significant tidal stretching of the star (*bottom left panel*), the star ultimately relaxes after losing 25% of its mass. At $\tilde{t} = 124$ (*bottom right panel*) the stellar mass that has settled back to within $\tilde{r} = 2$ of the stellar core rotates at 20% of the centrifugal breakup velocity. The moment of inertia of the mass within $\tilde{r} = 2$ is $\tilde{I} = 0.45$, more than twice its initial value. [*See the electronic edition of the Journal for a color version of this figure.*]

very deep collisions ($\tilde{r}_p \sim 0.5$; see Figs. 3 and 4), albeit with a significant mass loss. One concern when considering penetrating collisions by compact remnants is the energy release by nuclear reactions near the surface of the impactor. Różyczka et al. (1989) and Ruffert & Müller (1990) find that nuclear reactions probably do not play a significant role even in parabolic head-on collisions between low-mass stars and white dwarfs. We will assume that stars can survive collisions down to $\tilde{r}_p = 0.5$ even when the impactor is a compact object.

3.2.4. *The Survival Probability*

In an environment that is dense enough for efficient tidal spin-up there is also a nonnegligible probability for destructive head-on collisions. Our estimate of $\Delta\tilde{\Omega}$ implicitly assumed that the target star survives its full life span $\tilde{T}$. The Poissonian survival probability against collisions with $\tilde{r}_p < \tilde{r}_c$ over a time $\tilde{T}$ is

$$f_c = \exp\left(-\tilde{q}\tilde{T}\right), \tag{17}$$

where $\tilde{q}$ is the collision rate for collisions with $\tilde{r}_p < \tilde{r}_c$, which for a Maxwellian velocity DF is given by (e.g., Binney & Tremaine 1987)

$$\tilde{q} = 4\sqrt{\pi}\tilde{n}\tilde{\sigma}\tilde{r}_c^2\left(1 + \frac{1+\tilde{m}}{2\tilde{\sigma}^2\tilde{r}_c}\right), \tag{18}$$

where the second term expresses the enhancement due to gravitational focusing. Stars with low survival probability ($\tilde{q}\tilde{T} > 1$) will have a shorter effective lifetime for spin-up, $\sim\tilde{q}^{-1}$, and consequently $\delta\tilde{\Omega}$ will be reduced by a factor $\sim(\tilde{q}\tilde{T})^{-1/2}$ relative to that predicted by equation (7).

4. TIDAL SPIN-UP IN THE INNER GALACTIC CENTER

Up to this point our treatment of the tidal spin-up effect has been general. We now turn our attention to the specific case of the GC.

4.1. *The Stellar Velocity Distribution in the GC*

The effects of the stellar collisions depend critically on the relative velocity of the two colliding stars and their mass ratio. It is therefore important to understand the mass dependence of the velocity distribution. We are interested in particular in the case in which the stellar system around the

black hole has undergone two-body relaxation, as appears to be the situation in the GC (Alexander 1999).

Let $f_m(\epsilon)$ be the DF of stars of mass m ($m_1 \le m \le m_2$) as a function of specific energy in a spherical stellar system whose potential is dominated by a central BH, where $\epsilon = \Psi - v^2/2 > 0$, $\Psi = GM_{\rm BH}/r$, and $M_{\rm BH}$ is the mass of the BH. Bahcall & Wolf (1977) have shown that when such a system undergoes two-body relaxation, the DF has the following properties: $p_m \equiv d\ln f_m/d\ln\epsilon \sim$ constant to a good approximation, $p_{m_2} \simeq 1/4$, and $p_m/p_{m_2} \simeq m/m_2$ so that $0 \lesssim p_m \lesssim 1/4$. In this case $f_m(\epsilon) \propto \epsilon^{p_m}$ and the velocity dispersion $\sigma_m^2 = \langle v^2\rangle/3$ is

$$\sigma_m^2 = \left(\frac{1}{p_m + 5/2}\right)\frac{GM_{\rm BH}}{r} . \tag{19}$$

The velocity dispersion is almost independent of the stellar mass. The relative change in the value of σ_m^2 over the full mass range is only $\sim 10\%$ independently of the ratio m_2/m_1, in marked contrast with the wide spread of velocities expected in the case of equipartition in which $\sigma_m^2 \propto m^{-1}$. The reason why the relaxed system does not reach equipartition can be understood by considering the fate of a massive star that is momentarily on a circular orbit. The orbital radius depends only on the specific energy. Equipartition works to equate the kinetic energy per star, thereby always reducing the specific energy of the massive stars and causing them to sink to ever lower orbits. This is analogous to the equipartition instability discussed by Spitzer (1969) in the context of a stellar cluster without a central BH, but where the fraction of mass in the massive stars is large enough to create a centrally concentrated subsystem.

The resulting distribution of the relative velocity $\boldsymbol{v}_2 = \boldsymbol{v}_a - \boldsymbol{v}_b$ between two stars of masses $m_1 \le m_a \le m_b \le m_2$ is given by

$$f((\boldsymbol{v}_2)) = \frac{1}{8\pi^3\Psi^{3/2}}\frac{\Gamma(5/2 + p_{m_a})\Gamma(5/2 + p_{m_b})}{\Gamma(1 + p_{m_a})\Gamma(1 + p_{m_b})} \times \int d^3u\left(1 - \frac{u^2}{2}\right)^{p_{m_a}}\left[1 - \frac{((\boldsymbol{u}) - (\boldsymbol{w}))^2}{2}\right]^{p_{m_b}} , \tag{20}$$

where $(\boldsymbol{u}) \equiv (\boldsymbol{v}_a)/\Psi^{1/2}$, $(\boldsymbol{w}) \equiv (\boldsymbol{v}_2)/\Psi^{1/2}$, and the integration is over the region $u < \sqrt{2}$ and $|(\boldsymbol{w}) - (\boldsymbol{u})| < \sqrt{2}$. This distribution is not very different from a Maxwellian DF with the same one-dimensional velocity dispersion σ. This can be seen in Figure 6, which compares the Maxwellian DF with the case in which both $p_{m_a} = p_{m_b} = 0$ (low-mass stars) and equation (20) simplifies to

$$f(v_2)dv_2 = \frac{\Gamma(5/2)^2}{24\pi} w^2(32\sqrt{2} - 24w + w^3)dw .$$

In particular, the two DFs have the same mean orbital energy

$$\langle E_o\rangle = 3\mu\sigma^2 . \tag{21}$$

We conclude that the velocity field in a relaxed stellar system very near a BH is well approximated by a Maxwellian velocity distribution where the one-dimensional velocity dispersion is independent of the stellar mass.

4.2. *The Stellar Population in the GC*

Stellar population synthesis models of the observed luminosity function averaged over the inner few parsecs of the GC (Alexander & Sternberg 1999) indicate that it is well described by a continuous star-forming population with a Miller-Scalo initial mass function (IMF; Miller & Scalo 1979) with masses in the range 0.1–125 $M_\odot$. The mean impactor mass (live stars and remnants) in this model is $\langle m\rangle = 0.5\ M_\odot$. In an isolated system the present-day mass function (PMF) preserves the IMF distribution for low-mass stars that are longer lived than the system but falls more rapidly for the shorter lived massive stars, so that over time the low-mass stars accumulate and take an ever larger fraction of the total stellar mass. However, the timescale for mass segregation in the GC, which is of the same order as the relaxation timescale, is only 3 Gyr (e.g., Alexander 1999). It is therefore reasonable to assume that the mass fraction of the very low mass stars in the inner GC is significantly lower than implied by continuous star formation.

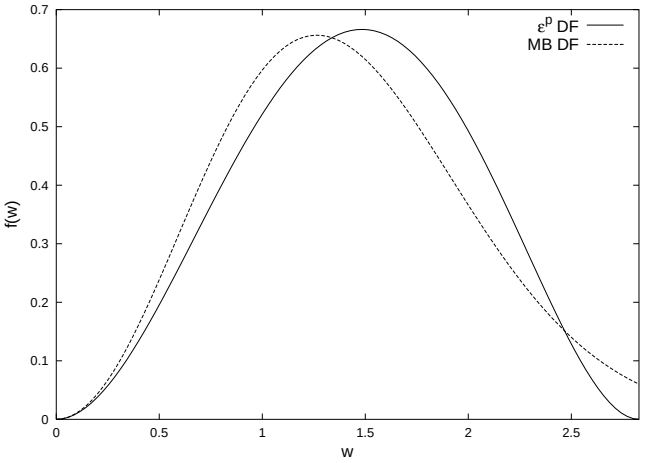

FIG. 6.—Comparison of the DFs of the relative stellar velocity ($w \equiv v_2/\Psi^{1/2}$) in a Maxwellian DF and in an ϵ^p DF of relaxed low-mass stars very near a black hole (Bahcall & Wolf 1977). Both DFs have the same one-dimensional velocity dispersion and the same mean orbital energy.

In view of the uncertainties in the low-mass end of the PMF, we do not attempt to construct a detailed mass function for the impactors in the innermost GC. Instead, we base it on the stellar synthesis model (Table 2) and take account of the mass segregation by assuming a Salpeter power-law PMF with a low-mass cutoff close to the mean impactor mass. The model parameters are listed in Table 3. The mean impactor mass in this model is $\langle m\rangle = 0.9\ M_\odot$. We carried out spot checks to verify that the exact values of the mass ranges and power-law indices do not affect the final results significantly. The one important assumption in this model is that the mass in the inner GC is not dominated

TABLE 2

STELLAR REMNANT MASS AS A FUNCTION OF INITIAL STELLAR MASS

Initial Mass Range ($M_\odot$)	Remnant Mass ($M_\odot$)	Mass Fraction
0.8–1.5	0.6	0.03
1.5–2.5	0.7	0.08
2.5–8	1.1	0.12
8–30	1.4	0.03
>30	10	0.01

NOTE.—Stellar remnant mass as a function of initial stellar mass (Meylan & Mayor 1991; Timmes, Woosley, & Weaver 1996) and its mass fraction in the continuous star-forming stellar population model for the GC (Alexander & Sternberg 1999).

TABLE 3

MODEL FOR THE IMPACTOR MASS FUNCTION IN THE INNER GC

Type	Mass Range ($M_\odot$)	α	Mass Fraction
MS	0.4–4.0	2.35	0.73
WD.....	0.7–1.1	0.0	0.23
NS.....	1.2–1.5	2.35	0.03
BH	7.0–12.0	2.35	0.01

NOTE.—A $df/dm \propto m^{-\alpha}$ mass distribution is assumed within the mass range.

by very low mass stars, which are inefficient in raising tides. More detailed modeling of the dynamical evolution of the inner GC will be required to verify this. The results for the tidal spin-up that are presented below can easily be scaled to other mass fraction ratios through equations (8) and (9).

We represent the mass distribution in the innermost GC by a stellar cusp of the form (§ 4.1; see also Alexander 1999)

$$\rho = 10^6 \left(\frac{r}{0.4 \text{ pc}} \right)^{-(3/2 + p_m)} M_\odot \text{ pc}^{-3} , \qquad (22)$$

and the one-dimensional velocity dispersion by equation (19). We set $p_m = 0$ to represent the typical low-mass impactors and assume $M_{\rm BH} = 2.6 \times 10^6 M_\odot$ (Genzel et al. 1997).

4.3. *Results*

We calculated the spin-up in the GC following the procedure outlined in the previous sections. To summarize, the calculation proceeded by a triple numeric integration: first, integration over the impactor mass function (Table 3); second, integration over $\tilde{r}_p$ from a suitably large distance down to the larger of $\tilde{r}_t$ (eq. [16]) and $\tilde{r}_p = 0.5$ where for $\tilde{r}_p < \tilde{r}_0 = 1$, $\Delta\tilde{\Omega}$ was held fixed to account for mass loss; and third, integration over $\tilde{E}_o$ from a suitable large value down to 0. Collisions that resulted in bound orbits (eq. [13]) were omitted from the sum. For each point in the integration, $\Delta\tilde{\Omega}$ was calculated (eq. [12]) with a nonlinear correction factor $C_{\rm NL} = 2$ and summed in quadrature, weighted by the differential rate (eq. [8]). We assumed that long after the collision $\tilde{I}$ recovers its initial value and that $\tilde{m}$ is unchanged.

Figure 7 shows the run of $\delta\tilde{\Omega}$ with distance from the BH in the GC for the model MS target star with $T = 10$ Gyr, as well as the separate contributions from collisions with white dwarfs (WDs), neutron stars (NSs), and stellar mass BHs. Figure 7 also shows that the survival probability is of order unity as close as 0.02 pc to the BH, and so the fact that it was not taken into account explicitly in the estimate of $\delta\tilde{\Omega}$ does not introduce a serious error. Interior to 0.02 pc the collisional destruction of MS stars is expected to flatten the cusp to an $r^{-1/2}$ configuration of marginally bound stars (Murphy, Cohn, & Duriden 1991; Alexander 1999). The stellar rotation falls only slowly with distance from the black hole and is at the level of $\delta\tilde{\Omega} \sim 0.1$–$0.3$ in the inner 0.3 pc. Most of the effect comes from collisions with MS stars and WDs. Field MS stars later than ~F5 are very slow rotators (Gray 1992). For $\sim 1 M_\odot$ stars these values of $\delta\tilde{\Omega}$ correspond to rotational velocities 20–60 times higher than normal (Table 1).

We carried out similar calculations for giant stars. We find that the spin-up is much smaller, $\delta\tilde{\Omega} \sim 0.01$–$0.02$, because of the much higher $\tilde{\sigma}$ and the shorter lifetime in the giant phase. This is similar to the rotational velocity of field giants later than ~G3, and thus tidal spin-up may increase their rotation to double the normal value.

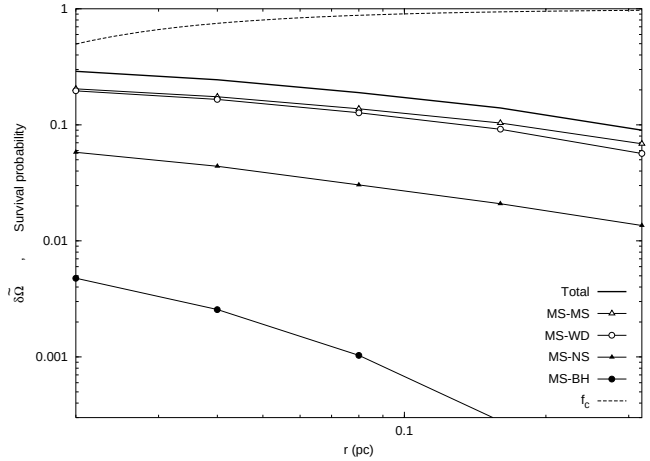

FIG. 7.—Mean stellar spin $\Delta\tilde{\Omega}$ of an MS star as a function of distance from the BH in the GC assuming a Salpeter PMF and the remnant mass fractions listed in Table 2. The survival probability against a destructive collision with $\tilde{r}_p < 0.5$ over 10 Gyr (eq. [17]) is also plotted for a mean impactor mass of $\langle m \rangle = 0.9 M_\odot$.

5. DISCUSSION AND SUMMARY

Dense stellar cusps around massive BHs are environments where stellar collisions are frequent and energetic. Hyperbolic head-on collisions may destroy the colliding stars, but they are rare. For every head-on collision there are many more close tidal encounters and grazing collisions. The cumulative effects of such encounters are more subtle. Energy and angular momentum are transferred from the orbit to the stars, during the flyby the stellar structure may be significantly disturbed by the tidal forces, and some mass may be lost. However, the stars survive the collision, and because of the high initial orbital energy, they rarely form a bound binary system. This is in contrast to the situation in dense globular clusters. The stellar dynamical and thermal relaxation timescales are very short relative to the stellar lifetime, and the star can radiate the excess energy quickly. It is harder to shed the excess angular momentum, since magnetic breaking operates on timescales of the order of the stellar lifetime. Thus, the direct long-term effects of the collision are increased rotation and possibly some mass loss and some mixing of the stellar envelope.

In this study we calculated the magnitude of the rotation that is built up in a random walk fashion as the star undergoes multiple hyperbolic tidal encounters. This is of interest because of the effects high rotation may have on the star's evolution and on its observed properties and because, unlike destructive collisions, the spin-up affects the entire stellar population and extends over a much larger volume of the galactic nucleus. Many, if not most, galaxies have a supermassive BH in their nucleus, and so high stellar rotation in galactic nuclei may be common.

Our approach to the problem was to use detailed stellar structure models to calculate, for the first time, the tidal coupling constants for arbitrary hyperbolic orbits in the linear regime of soft encounters. Because the tidal energy and angular momentum fall off as a high power of the periseparation, it was necessary to extend the calculation to the strongly nonlinear regime of grazing and penetrating

collisions. We carried out a suite of SPH simulations to study the qualitative behavior of such collisions and then conservatively extrapolated the exact linear calculations to the nonlinear regime by several simple prescriptions. The simulations indicated the following. (1) At periseparations closer than about twice the target star's radius, the linear results are smaller than the actual spin-up by a factor of at least 2. (2) Once mass loss becomes significant, the ejecta carry away a large fraction of the angular momentum that is extracted from the orbit, and therefore the spin-up saturates at its level just before the onset of mass loss. (3) Stars can survive deep collisions down to a periseparation of half the target star's radius. (4) A simple tidal disruption criterion for hyperbolic encounters can roughly indicate the point where the fractional mass loss increases to order unity.

We calculated the spin-up of stars in the inner parsec of the Galactic center, which is of special interest because of the high quality and wealth of details of the observed stellar data. We find that over 10 Gyr, $\sim 1\ M_\odot$ MS stars in the inner 0.3 pc are stochastically spun-up to 10%–30% of the centrifugal breakup velocity (20–60 times higher than is usual for such stars in the field). This effect decreases only weakly with distance from the BH because the increased tidal coupling at lower collision velocities largely compensates for the decrease in the collision rate at lower stellar densities. We estimated also the stellar survival probability against head-on collisions over 10 Gyr and found that it was significantly large even very close to the center. The fact that the spin-up is roughly constant over the volume of the inner GC implies that no large error was introduced by neglecting the fact that stars on noncircular orbits sample a varying stellar density over their lifetime. The spin-up of giant stars over the giant phase is much smaller, of order 1%–2% of the centrifugal breakup velocity (doubling the rotation that is usual for such stars in the field). The effect is smaller because of their short lifetime and because of the large ratio between the collision velocity and the stellar escape velocity, which decreases the tidal coupling.

Tidal spin-up is inefficient in globular clusters, where in the absence of a central BH the velocity dispersion is so low that a close encounter usually extracts enough energy from the orbit for tidal capture. The spin-up by more distant hyperbolic encounters is negligibly small because of the steep $\Delta\tilde{\Omega} \sim \tilde{r}_p^{-4.5}$ falloff (eq. [5]).

These results suggest that stochastic spin-up is an important stellar effect in BH cusps. However, several caveats apply. In our treatment we neglected the effects of magnetic breaking, which, although slow, may be effective over 10 Gyr. As a very crude estimate, consider the Sun, for which the halving time of rotation due to magnetic breaking is $\sim 5 \times 10^9$ yr (Brandt 1966). The spin-up is dominated by the closest encounter, which occurs on average at $\tilde{T}/2$, and so on average half of the acquired rotation will be lost as a result of magnetic breaking by $\tilde{T} = 10$ Gyr. This estimate is obviously quite uncertain, since the spin-up and the cumulative mass loss in the course of many collisions are likely to play some role in the magnetic breaking process. Unfortunately, at present the details of this process cannot be modeled with any certainty. Our results depend on the validity of our extrapolation to the nonlinear regime. A real star is not well represented by an ideal gas $n = 1.5$ polytrope, and more realistic and extensive hydrodynamical simulations, including the effects of radiation and nuclear burning, will be needed to verify our results. We note, however, that the $n = 1.5$ polytrope model is significantly less bound than the realistic stellar models (Table 1). This implies that our estimates for the minimal periseparation and the tidal radius may be overly conservative. Nevertheless, because a smaller binding energy, larger tidal coupling coefficients (Fig. 1), and a larger moment of inertia go hand in hand, the spin-up ($\Delta\tilde{\Omega} \sim T_l/\tilde{I}$) is less sensitive to the details of the stellar structure than any of these quantities separately. Another uncertainty in applying our results to any specific system, such as the GC, lies in modeling the PMF of the impactors. Generally, mass segregation will work toward increasing the spin-up effect by pushing the ineffective low-mass projectiles out of the central region. Dynamical models of the evolution of the galactic nucleus are required to put this on a quantitative footing.

Detailed predictions for the observational consequences of high rotation are outside the scope of this work. We limit our comments on this matter to noting that rotation lowers the effective temperature and luminosity of a star (Kippenhahn, Meyer-Hofmeister, & Thomas 1970) but does not significantly affect the spectral classification of a star until it is close to breakup (Gray 1992). The long-term effects of rotation on stellar evolution may be more significant. We calculated the effective angular velocity, assuming solid body rotation. The actual distribution of angular momentum could become stratified over time and lead to rotational support of the core (Vandenberg et al. 1998) or to the replenishment of the hydrogen in the core by large-scale deep mixing (Sweigart 1997). These effects will manifest themselves in the giant phase of the stars. Finally, we note that even in the GC only the giant stars can be presently observed. Rotational broadening in the giant spectra may be marginally detectable with high-resolution spectroscopy and could bolster the case for the existence of an underlying very dense population of faint stars.

To summarize, we have shown that MS stars in a substantial volume of the dense cusps around massive black holes are likely to rotate at a significant fraction of the centrifugal breakup velocity as a result of stochastic spin-up by hyperbolic tidal encounters.

We are grateful to P. Demarque for providing us with the stellar structure model of the αUMa giant.

APPENDIX A

LINEAR TIDAL COUPLING COEFFICIENTS FOR HYPERBOLIC ORBITS

Following the formalism of Press & Teukolsky (1977), the linear tidal coupling coefficients are expressed as

$$T_l(\eta) = 2\pi^2 \sum_n |Q_{nl}|^2 \sum_{m=-l}^{l} |K_{nlm}|^2 , \tag{A1}$$

TABLE 4

MODE FREQUENCIES AND OVERLAP INTEGRALS FOR THE SOLAR MODEL OF CHRISTENSEN-DALSGAARD ET AL. (1996)

	$l = 2$		$l = 3$		$l = 4$		$l = 5$	
MODE	$\tilde{w}_{nl}^2$	$\lvert Q_{nl}\rvert$	$\tilde{w}_{nl}^2$	$\lvert Q_{nl}\rvert$	$\tilde{w}_{nl}^2$	$\lvert Q_{nl}\rvert$	$\tilde{w}_{nl}^2$	$\lvert Q_{nl}\rvert$
p_6	1.28 (+2)	2.38 (−2)	1.39 (+2)	1.12 (−2)	1.49 (+2)	5.39 (−3)	1.59 (+2)	2.74 (−3)
p_5	9.70 (+1)	3.26 (−2)	1.06 (+2)	1.58 (−2)	1.14 (+2)	8.00 (−3)	1.23 (+2)	4.28 (−3)
p_4	7.02 (+1)	4.67 (−2)	7.76 (+1)	2.34 (−2)	8.48 (+1)	1.22 (−2)	9.18 (+1)	6.82 (−3)
p_3	4.79 (+1)	6.85 (−2)	5.36 (+1)	3.48 (−2)	5.90 (+1)	1.91 (−2)	6.45 (+1)	1.14 (−2)
p_2	2.95 (+1)	1.06 (−1)	3.33 (+1)	5.61 (−2)	3.72 (+1)	3.32 (−2)	4.12 (+1)	2.16 (−2)
p_1	1.70 (+1)	1.47 (−1)	1.82 (+1)	9.18 (−2)	2.01 (+1)	6.36 (−2)	2.23 (+1)	4.66 (−2)
f.....	1.39 (+1)	1.39 (−1)	1.65 (+1)	5.54 (−2)	1.77 (+1)	8.62 (−3)	1.84 (+1)	7.56 (−4)
g_1	9.12 (+0)	4.58 (−2)	1.17 (+1)	8.47 (−3)	1.35 (+1)	4.80 (−3)	1.47 (+1)	2.40 (−3)
g_2	6.92 (+0)	1.13 (−1)	8.94 (+0)	4.46 (−2)	1.08 (+1)	1.64 (−2)	1.23 (+1)	7.29 (−3)
g_3	5.11 (+0)	1.07 (−1)	7.02 (+0)	8.99 (−2)	8.58 (+0)	3.81 (−2)	1.00 (+1)	1.56 (−2)
g_4	3.84 (+0)	8.31 (−2)	5.81 (+0)	1.10 (−1)	7.13 (+0)	1.00 (−1)	8.35 (+0)	4.85 (−2)
g_5	2.92 (+0)	5.66 (−2)	4.75 (+0)	7.20 (−2)	6.35 (+0)	1.04 (−1)	7.51 (+0)	1.29 (−1)
g_6	2.31 (+0)	3.91 (−2)	3.84 (+0)	4.36 (−2)	5.38 (+0)	4.76 (−2)	6.76 (+0)	5.20 (−2)
g_7	1.82 (+0)	2.77 (−2)	3.13 (+0)	2.90 (−2)	4.45 (+0)	2.73 (−2)	5.76 (+0)	2.31 (−2)
g_8	1.49 (+0)	1.99 (−2)	2.59 (+0)	2.04 (−2)	3.76 (+0)	1.84 (−2)	4.93 (+0)	1.48 (−2)
g_9	1.23 (+0)	1.44 (−2)	2.19 (+0)	1.47 (−2)	3.20 (+0)	1.30 (−2)	4.24 (+0)	1.03 (−2)
g_{10}	1.04 (+0)	1.07 (−2)	1.85 (+0)	1.12 (−2)	2.76 (+0)	1.02 (−2)	3.69 (+0)	8.20 (−3)

where Q_{nl} are overlap integrals that depend only on the stellar structure. The orbit enters in the term

$$K_{nlm} = \frac{W_{lm}}{\pi}\left(\frac{\tilde{r}_p^3}{1+\tilde{m}}\right)^{1/2}(1+e)^{-l+1/2}\int_0^{\phi_{\max}} d\phi(1+e\cos\phi)^{l-1}\cos\left[\tilde{\omega}_{nl}\tilde{t}(\phi)+m\phi\right], \tag{A2}$$

where $\tilde{\omega}_{nl}$ is the frequency of the mode, ϕ is the angular position of the impactor in a coordinate system centered on the target star ($\phi = 0$ at periastron),

$$\phi_{\max} = \arccos\left(\frac{1}{e}\right), \tag{A3}$$

and

$$W_{lm} = (-1)^{(l+m)/2}\frac{\{[4\pi/(2l+1)](l-m)!(l+m)!\}^{1/2}}{2^l[(l-m)/2]![(l+m)/2]!}. \tag{A4}$$

The time along the hyperbolic orbit as a function of the angle ϕ is given by

$$\tilde{t}(\phi) = \frac{(1+e)^{3/2}\tilde{r}_p^{3/2}}{(1+\tilde{m})^{1/2}}\left\{\frac{\sin\phi}{1+e\cos\phi}\frac{e}{e^2-1} - (e^2-1)^{-3/2}\log\left[\frac{e+\cos\phi+(e^2-1)^{1/2}\sin\phi}{1+e\cos\phi}\right]\right\}. \tag{A5}$$

Tables 4 and 5 list the mode frequencies and the overlap integrals for the solar and giant models that we investigate in this work. The classification of the giant modes is complicated by the large value of the Brunt-Väisälä frequency in the core, compared to the f-mode frequencies, thereby giving rise to a mix of p- and g-mode behavior. The corresponding values for ideal gas polytropes with $n = 1.5$, 2, and 3 are given in Lee & Ostriker (1986).

TABLE 5

MODE FREQUENCIES AND OVERLAP INTEGRALS FOR THE GIANT MODEL OF GUENTHER ET AL. (2000)

	$l = 2$		$l = 3$		$l = 4$	
MODE	$\tilde{w}_{nl}^2$	$\lvert Q_{nl}\rvert$	$\tilde{w}_{nl}^2$	$\lvert Q_{nl}\rvert$	$\tilde{w}_{nl}^2$	$\lvert Q_{nl}\rvert$
p_8	4.28 (+1)	1.25 (−2)	4.53 (+1)	1.62 (−2)	4.83 (+1)	1.86 (−2)
p_7	3.66 (+1)	1.66 (−2)	3.40 (+1)	2.82 (−2)	3.67 (+1)	3.18 (−2)
p_6	3.08 (+1)	2.29 (−2)	2.21 (+1)	6.09 (−2)	3.15 (+1)	4.12 (−2)
p_5	2.19 (+1)	4.35 (−2)	1.60 (+1)	1.02 (−1)	2.62 (+1)	5.86 (−2)
p_4	1.45 (+1)	8.40 (−2)	1.11 (+1)	1.66 (−1)	1.68 (+1)	1.13 (−1)
p_3	1.27 (+1)	1.05 (−1)	9.24 (+0)	2.47 (−1)	1.01 (+1)	2.27 (−1)
p_2	8.12 (+0)	2.36 (−1)	6.55 (+0)	1.26 (−1)	6.81 (+0)	3.59 (−2)
p_1	6.10 (+0)	2.68 (−1)	4.45 (+0)	9.06 (−2)	5.02 (+0)	3.42 (−2)
f	3.57 (+0)	1.84 (−1)	3.39 (+0)	8.86 (−2)	2.19 (+0)	3.69 (−2)

REFERENCES

Alexander, T. 1999, ApJ, 520, 137
Alexander, T., & Sternberg, A. 1999, ApJ, 520, 137
Bahcall, J. N., & Wolf, R. A. 1977, ApJ, 216, 883
Binney, J., & Tremaine, S. 1987, in Galactic Dynamics (Princeton: Princeton Univ. Press), 541
Brandt, J. C. 1966, ApJ, 144, 1221
Carr, J. S., Sellgren, K., & Balachandran, S. C. 2000, ApJ, 530, 307
Christensen-Dalsgaard, J., et al. 1996, Science, 272, 1286
Davies, M. B., Benz, W., & Hills, J. G. 1991, ApJ, 381, 449
Genzel, R., Eckart, A., Ott, T., & Eisenhauer, F. 1997, MNRAS, 291, 21
Ghez, A. M., Klein, B. L., Morris, M., & Becklin, E. E. 1998, ApJ, 509, 678
Gingold, R. A., & Monaghan, J. J. 1977, MNRAS, 181, 375
Goldreich, P., & Nicholson, P. D. 1989, ApJ, 342, 1079
Gray, D. F. 1992, in The Observation and Analysis of Stellar Photospheres (2d ed.; Cambridge: Cambridge Univ. Press), 386–396
Guenther, D. B., Demarque, P., Busazi, D., Catanzarite, J., Conrow, T., & Kreidl, T. 2000, ApJ, 530, L45
Hernquist, L. 1993, ApJ, 404, 717
Hernquist, L., & Katz, N. 1989, ApJS, 70, 419
Katz, N., Weinberg, D. H., & Hernquist, L. 1996, ApJS, 105, 19
Kippenhahn, R., Meyer-Hofmeister, E., & Thomas, H. C. 1970, A&A, 5, 155
Kumar, P., & Quataert, E. J. 1998, ApJ, 493, 412
Lang, K. R. 1991, in Astrophysical Data: Planets and Stars (New York: Springer), 138
Lee, H.-M., & Ostriker, J. P. 1986, ApJ, 310, 176
Lucy, L. 1977, AJ, 82, 1013
Magorrian, J., et al. 1998, AJ, 115, 2285
Meylan, G., & Mayor, M. 1991, A&A, 250, 113
Miller, G. E., & Scalo, J. M. 1979, ApJS, 41, 513
Monaghan, J. J., & Lattanzio, J. C. 1985, A&A, 149, 135
Murphy, B. W., Cohn, H. N., & Durisen, R. H. 1991, ApJ, 370, 60
Press, W. H., & Teukolsky, S. A. 1977, ApJ, 213, 183
Ramirez, S. V., et al. 2000, ApJ, 537, 205
Rasio, F. A., & Shapiro, S. L. 1991, ApJ, 377, 559
Różyczka, M., Yorke, H. W., Bodenheimer, P., Müller, E., & Hashimoto, M. 1989, A&A, 208, 69
Ruffert, M., & Müller, E. 1990, A&A, 238, 116
Schaerer, D., Charbonnel, C., Meynet, G., Maeder, A., & Schaller, G. 1993, A&AS, 102, 339
Sills, A., Pinsonneault, M. H., & Terndrup, D. M. 2000, ApJ, 534, 335
Spitzer, L. 1969, ApJ, 158, L139
Sweigart, A. V. 1997, ApJ, 474, L23
Timmes, F. X., Woosley, S. E., & Weaver, T. A. 1996, ApJ, 457, 834
Vandenberg, D. A., Larson, A. M., & De Propris, R. 1998, PASP, 110, 98
Young, P. 1980, ApJ, 242, 1232
Zahn, J.-P. 1989, A&A, 220, 112
Zombeck, M. V. 1990, in Handbook of Space Astronomy and Astrophysics (2d ed.; Cambridge: Cambridge Univ. Press), 68